Spectrochimica Acta Part A: Molecular and Biomolecular Spectroscopy 122 (2014) 598–608

Contents lists available at ScienceDirect

Spectrochimica Acta Part A: Molecular and Biomolecular Spectroscopy

journal homepage: www.elsevier.com/locate/saa

Coordination modes of bidentate lornoxicam drug with some transition metal ions. Synthesis, characterization and in vitro antimicrobial and antibreastic cancer activity studies

Walaa H. Mahmoud, Gehad G. Mohamed *, Maher M.I. El-Dessouky

Chemistry Department, Faculty of Science, Cairo University, Giza 12613, Egypt

HIGHLIGHTS

- Mononuclear complexes of lornoxicam drug with transition metal ions were prepared.
- The bonding and stereochemistry were deduced from elemental and spectroscopic data.
- The activation kinetic parameters are calculated using DTG curves.
- The metal complexes showed antimicrobial inhibition capacity comparable to LOR ligand.
- The Cr(III), Fe(II) and Cu(II) complexes have high anticancer activity against MCF7.

GRAPHICAL ABSTRACT

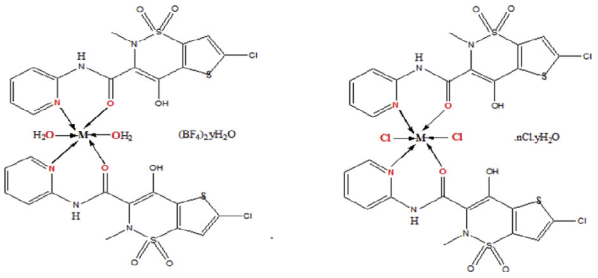

M = Co(II), Cu(II) and Zn(II) complexes M = Cr(III), Mn(II), Fe(III) and Ni(II) complexes

ARTICLE INFO

Article history:
Received 19 August 2013
Received in revised form 19 October 2013
Accepted 10 November 2013
Available online 21 November 2013

Keywords:
Lornoxicam
Metal complexes
Spectroscopy
TG–DTG
Antimicrobial activity
Antitumor agents

ABSTRACT

The NSAID lornoxicam (LOR) drug was used for complex formation reactions with different metal salts like Cr(III), Mn(II), Fe(III) and Ni(II) chlorides and Fe(II), Co(II), Cu(II) and Zn(II) borates. Mononuclear complexes of these metals are obtained that coordinated to NO sites of LOR ligand molecule. The nature of bonding and the stereochemistry of the complexes have been deduced from elemental analyses, IR, UV–Vis, ^{1}H NMR, mass, electronic spectra, magnetic susceptibility and ESR spectral studies, conductivity measurements, thermogravimetric analyses (TG–DTG) and further confirmed by X-ray powder diffraction. The activation thermodynamic parameters are calculated using Coats–Redfern and Horowitz–Metzger methods. The data show that the complexes have composition of ML_2 type except for Fe(II) where the type is $[ML_3]$. The electronic absorption spectral data of the complexes suggest an octahedral geometry around the central metal ion for all the complexes. The antimicrobial data reveals that LOR ligand in solution show inhibition capacity less or sometimes more than the corresponding complexes against all the species under study. In order to establish their future potential in biomedical applications, anticancer evaluation studies against standard breast cancer cell lines (MCF7) was performed using different concentrations. The obtained results indicate high inhibition activity for Cr(III), Fe(II) and Cu(II) complexes against breast cancer cell line (MCF7) and recommends them for testing as antitumor agents.

Introduction

Medical inorganic chemistry is becoming an emerging area of research due to the demand for new biologically active compounds. Various investigations have proved that binding of a drug to a metallo element enhances its activity and in some cases, the complex possesses even more healing properties than the parent drug [1]. Oxicam ligands are wide spread among coordination compounds and are important components of biological transition metal complexes [2]. The oxicam group of nonsteroidal anti-inflammatory drugs (NSAIDs) has emerged as highly effective class

* Corresponding author. Tel.: +20 235676896.
E-mail address: ggenidy@hotmail.com (G.G. Mohamed).

1386-1425/$ - see front matter © 2013 Elsevier B.V. All rights reserved.
http://dx.doi.org/10.1016/j.saa.2013.11.069

of drugs against various arthritic conditions and post-operative inflammation. Recently several other functions of these groups of drugs have been identified which included chemoprevention, chemosuppression, UV-sensitization, UV-protection, etc. These drugs are also found to be very good anti-oxidants. Most oxicams are congeneric compounds generated by the concept of isosteric substitution in drug design [3]. Oxicam family, piroxicam, tenoxicam, meloxicam, lornoxicam and isoxicam, are widely used in inflammatory and painful diseases of rheumatic and non-rheumatic origin. They are potent inhibitors of cyclo-oxygenase in vitro and in vivo, thereby decreasing the synthesis of prostaglandins, prostacyclin, and thromboxane products [3,4].

New studies from the last years revealed that in addition to arthritis and pain, cancer and neurodegenerative diseases like Alzheimer's disease could potentially be treated with COX-2 inhibitors [4]. The direct interaction of NSAIDs and their metal complexes with DNA is of interest since their anticancer activity may be explained [5].

Lornoxicam (LOR) is a non-steroidal anti-inflammatory drug (Fig. 1) of the oxicam class with analgesic, anti-inflammatory and antipyretic properties. It is available in oral and parenteral formulations. It is used for inflammatory disease of the joints, osteoarthritis, pain following surgery and pain in the lower back and hip which travels down the back of the thigh into the leg (sciatica). LOR differs from other oxicam compounds in its potent inhibition of prostaglandin biosynthesis, a property that explains the particularly pronounced efficacy of the drug [6].

The goal in this research was to explore the probability to extend the pharmacological profile of lornoxicam (LOR) drug, in order to disk over new properties such as antimicrobial and anti-cancer activity and to prepare new complexes of LOR with essential metal ions, which probably would exhibit different biological behaviour compared to the parent drug [4]. The structures of the metal complexes were characterized by elemental analyses, IR, ^{1}H NMR, ESR, UV–Vis, XRD, conductivity, mass spectra and magnetic susceptibility measurements at room temperature, thermal analyses as well as some results of bioactivity tests are also included.

Experimental

Materials and reagents

All chemicals used were of the analytical reagent grade (AR), and of highest purity available. The chemicals used included lornoxicam drug (supplied from National Organization for Drug Control and Research), $CrCl_3{\cdot}6H_2O$ and $MnCl_2{\cdot}2H_2O$ (Sigma), $NiCl_2{\cdot}6H_2O$ (BDH), $FeCl_3{\cdot}6H_2O$ (Prolabo), $Fe(BF_4)_2{\cdot}6H_2O$ and $Co(BF_4)_2{\cdot}6H_2O$ (Aldrich), $Cu(BF_4)_2{\cdot}6H_2O$ (Merck) and $Zn(BF_4)_2$ (Strem Chemicals). Organic solvents were spectroscopic pure from BDH included ethanol, diethyl ether and dimethyl formamide. Hydrogen peroxide, sodium chloride, sodium carbonate and sodium hydroxide (A.R.) were used.

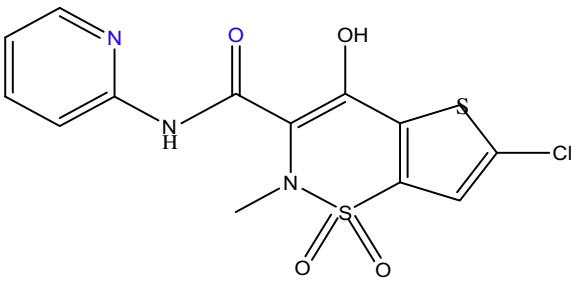

Fig. 1. The structure of lornoxicam drug.

Human tumor cell line (Brest cell) was obtained frozen in liquid nitrogen (−180 °C) from the American Type Culture Collection and was maintained in the National Cancer Institute, Cairo, Egypt, by serial sub-culturing.

Solutions

A fresh stock solution of 1×10^{-3} M of LOR (0.372 g/L) was prepared in the appropriate volume of absolute ethanol and DMF by a ratio (1:5 v/v ethanol:DMF). Dimethylsulphoxide (DMSO) (Sigma Chemical Co., St. Louis, Mo, and USA): It was used in cryopreservation of cells. RPMI-1640 medium (Sigma Chemical Co., St. Louis, Mo, and USA) was used. The medium was used for culturing and maintenance of the human tumor cell line. The medium was supplied in a powder form. It was prepared as follows: 10.4 g medium was weighed, mixed with 2 g sodium bicarbonate, completed to 1 L with distilled water and shaked carefully till complete dissolution. The medium was then sterilized by filtration in a Millipore bacterial filter (0.22 μm). The prepared medium was kept in a refrigerator (4 °C) and checked at regular intervals for contamination. Before use, the medium was warmed at 37 °C in a water bath and supplemented with penicillin/streptomycin and FBS.

Sodium bicarbonate (Sigma Chemical Co., St. Louis, Mo, USA) was used for the preparation of RPMI-1640 medium. 0.05% Isotonic Trypan blue solution (Sigma Chemical Co., St. Louis, Mo, USA) was prepared in normal saline and was used for viability counting. 10% Fetal Bovine Serum (FBS) (heat inactivated at 56 °C for 30 min), 100 units/ml Penicillin and 2 mg/ml Streptomycin were supplied from Sigma Chemical Co., St. Louis, Mo, USA and were used for the supplementation of RPMI-1640 medium prior to use. 0.025% (w/v) Trypsin (Sigma Chemical Co., St. Louis, Mo, USA) was used for the harvesting of cells. 1% (v/v) Acetic acid (Sigma Chemical Co., St. Louis, Mo, USA) was used for dissolving the unbound SRB dye. 0.4% Sulphorhodamine-B (SRB) (Sigma Chemical Co., St. Louis, Mo, USA) dissolved in 1% acetic acid was used as a protein dye. A stock solution of trichloroacetic acid (TCA, 50%, Sigma Chemical Co., St. Louis, Mo, USA) was prepared and stored. 50 μl of the stock was added to 200 μl RPMI-1640 medium/well to yield a final concentration of 10% used for protein precipitation. 100% Isopropanol and 70% ethanol were used. Tris base 10 mM (pH 10.5) was used for SRB dye solubilization. 121.1 g of tris base was dissolved in 1000 ml of distilled water and pH was adjusted by HCl acid (2 M).

Measurements

Microanalyses of carbon, hydrogen and nitrogen were carried out at the Microanalytical Center, Cairo University, Egypt, using CHNS-932 (LECO) Vario Elemental Analyzer. Analyses of the metals followed the dissolution of the solid complexes in concentrated HNO_3, neutralizing the diluted aqueous solutions with ammonia and titrating the metal solutions with EDTA. FT-IR spectra were recorded on a Perkin-Elmer 1650 spectrometer (4000–400 cm^{-1}) in KBr pellets. Electronic spectra were recorded at room temperature on a Shimadzu 3101pc spectrophotometer as solutions in ethanol. ^{1}H NMR spectra, as a solution in DMSO-d_6, were recorded on a 300 MHz Varian-Oxford Mercury at room temperature using TMS as an internal standard. Electron spin resonance spectra were also recorded on JES-FE2XG ESR spectrophotometer at Microanalytical Center, Tanta University.

Mass spectra were recorded by the EI technique at 70 eV using MS-5988 GS-MS Hewlett–Packard instrument at the Microanalytical Center, National Center for Research, Egypt. The molar magnetic susceptibility was measured on powdered samples using the Faraday method. The diamagnetic corrections were made by Pascal's constant and $Hg[Co(SCN)_4]$ was used as a calibrant. Molar conductivities of 10^{-3} M solutions of the solid complexes in DMF

were measured using Jenway 4010 conductivity meter. The thermogravimetric analyses (TG and DTG) of the solid complexes were carried out from room temperature to 800 °C using a Shimadzu TG-50H thermal analyzer. The X-ray powder diffraction analyses were carried out using Philips Analytical X-ray BV, diffractometer type PW 1840. Radiation was provided by copper target (Cu anode 2000 W) high intensity X-ray tube operated at 40 KV and 25 mA. Divergence and the receiving slits were 1 and 0.2, respectively. The antimicrobial activities were carried out at the Microanalytical Center, Cairo University, Egypt. The anticancer activity was performed at the National Cancer Institute, Cancer Biology Department, Pharmacology Department, Cairo University. The optical density (O.D.) of each well was measured spectrophotometrically at 564 nm with an ELIZA microplate reader (Meter tech. Σ 960, USA).

Synthesis of LOR -metal complexes

Ethanolic solution of lornoxicam (0.4 g, 1.07 mmol) and hydrated metal salts (0.143 g Cr(III), 0.087 g Mn(II), 0.181 g Fe(II), 0.145 g Fe(III), 0.182 g Co(II), 0.127 g Ni(II), 0.186 g Cu(II) and 0.129 g Zn(II), 1.0 mmol) was heated under reflux for 2–3 h. The precipitates were filtered off, washed with ethanol followed by diethyl ether and dried in a vacuum desiccator over anhydrous $CaCl_2$. The physical and analytical data of the isolated complexes are listed in Table 1. The complexes have high melting points and they are found to be air stable. The ligand is soluble in common organic solvents and all the complexes are freely soluble in DMF and DMSO but slightly soluble in methanol and ethanol and insoluble in water.

Spectrophotometric studies

The absorption spectra were recorded for 10^{-4} M solutions of the LOR free ligand and its binary metal complexes dissolved in DMF. The spectra were scanned within the wavelength range from 200 to 700 nm.

Pharmacology

Antimicrobial activity

A filter paper disk (5 mm) was transferred into 250 ml flasks containing 20 ml of working volume of tested solution (100 mg/ml). All flasks were autoclaved for 20 min at 121 °C. LB agar media surfaces were inoculated with four investigated bacteria (gram positive bacteria: *Bacillus subtilis* and *Staphylococcus aureus*, gram negative bacteria: *Neisseria gonorrhoeae* and *Escherichia coli*) and one strain of fungi (*Candida albicans*) by diffusion agar technique, then, transferred to a saturated disk with a tested solution in the center of Petri dish (agar plates). All the compounds were placed at 4 equidistant places at a distance of 2 cm from the center in the inoculated Petriplates. DMSO served as control. Finally, all these Petri dishes were incubated at 25 °C for 48 h where clear or inhibition zones were detected around each disk. Control flask of the experiment was designed to perform under the same condition described previously for each microorganism but with dimethylformamide solution only and by subtracting the diameter of inhibition zone resulting with dimethylformamide from that obtained in each case, so antibacterial activity could be calculated [7]. Amikacin and ketoconozole were used as reference compounds for antibacterial and antifungal activities, respectively. All experiments were performed as triplicate and data plotted were the mean value.

Anticancer activity

Potential cytotoxicity of the compounds was tested using the method of Skehan and Storeng [8]. Cells were plated in 96-multiwell plate (104 cells/well) for 24 h before treatment with the compounds to allow attachment of cell to the wall of the plate. Different concentrations of the compounds under investigation (0, 5, 12.5, 25, 50 and 100 μg/ml) were added to the cell monolayer triplicate wells were prepared for each individual dose. The monolayer cells were incubated with the compounds for 48 h at 37 °C and in 5% CO_2 atmosphere. After 48 h, cells were fixed, washed and stained with SRB stain. Excess stain was washed with acetic acid and attached stain was recovered with tris–EDTA buffer. The optical density (O.D.) of each well was measured spectrophotometrically at 564 nm with an ELIZA microplate reader and the mean background absorbance was automatically subtracted and mean values of each drug concentration was calculated. The relation between surviving fraction and drug concentration is plotted to get the survival curve of Breast tumor cell line for each compound.

Calculation:

The percentage of cell survival was calculated as follows:

$$\text{Survival fraction} = \text{O.D.(treated cells)}/\text{O.D.(control cells)}.$$

The IC_{50} values (the concentrations of thymoquinone required to produce 50% inhibition of cell growth). The experiment was repeated 3 times for MCF7 cell line.

Table 1
Analytical and physical data of LOR metal complexes.

Compound (Molecular Formula)	Colour (%yield)	M.p. (°C)	% Found (Calcd.)					$\mu_{eff.}$ (B.M.)	$\Lambda_m\ \Omega^{-1}\ mol^{-1}\ cm^2$
			C	*H*	*N*	*S*	*M*		
$[Cr(LOR)_2Cl_2]Cl$ ($C_{26}H_{20}Cl_5CrN_6O_8S_4$)	Green (93)	220	34.53 (34.61)	2.25 (2.21)	9.32 (9.22)	14.17 (14.20)	5.83 (5.77)	3.30	85
$[Mn(LOR)_2Cl_2]H_2O$ ($C_{26}H_{22}Cl_4N_6O_9S_4Mn$)	Yellow (83)	230	35.73 (35.15)	2.88 (2.84)	9.55 (9.46)	14.60 (14.42)	6.59 (6.20)	5.26	16
$[Fe(LOR)_3](BF_4)_2$ ($C_{39}H_{30}B_2Cl_3F_8FeN_9O_{12}S_6$)	Brown (87)	195	34.99 (34.79)	2.29 (2.23)	9.33 (9.37)	14.50 (14.27)	4.12 (4.16)	5.01	120
$[Fe(LOR)_2Cl_2]Cl{\cdot}2H_2O$ ($C_{26}H_{24}Cl_5FeN_6O_{10}S_4$)	Brown (92)	190	31.56 (31.90)	2.79 (2.45)	8.73 (8.59)	13.26 (13.09)	5.74 (5.73)	5.33	89
$[Co(LOR)_2(H_2O)_2](BF_4)_2{\cdot}3H_2O$ ($C_{26}H_{30}B_2Cl_2CoF_8N_6O_{13}S_4$)	Orange (86)	210	29.78 (29.25)	3.01 (2.81)	7.43 (7.88)	11.98 (12.00)	5.51 (5.48)	5.39	130
$[Ni(LOR)_2Cl_2]$ ($C_{26}H_{20}Cl_4N_6NiO_8S_4$)	Green (89)	215	35.88 (35.71)	2.43 (2.29)	9.50 (9.61)	14.72 (14.65)	6.81 (6.75)	3.23	20
$[Cu(LOR)_2(H_2O)_2](BF_4)_2{\cdot}4H_2O$ ($C_{26}H_{32}B_2Cl_2CuF_8N_6O_{14}S_4$)	Brown (93)	250	28.80 (28.65)	2.84 (2.94)	7.89 (7.71)	11.90 (11.75)	5.83 (5.83)	1.72	145
$[Zn(LOR)_2(H_2O)_2](BF_4)_2{\cdot}H_2O$ ($C_{26}H_{26}B_2Cl_2F_8N_6O_{11}S_4Zn$)	Yellow (95)	200	30.13 (30.09)	2.69 (2.50)	8.68 (8.11)	12.19 (12.35)	6.28 (6.27)	Diam.	140

Result and discussion

Microanalysis

The results of elemental analyses (C, H, N and S) with molecular formula and the melting points are presented in Table 1. As borne out by the elemental analysis data, the composition of the present complexes was found to be of 1:2 metal:LOR ligand stoichiometry and agree with the proposed formula of ML_2 type for all complexes except for Fe(II) complex, it is found to be 1:3 metal:LOR ligand stoichiometry. All the complexes were stable at room temperature and possessed good keeping qualities. They were non-hygroscopic solids and insoluble in ethanol and water but soluble in DMF and DMSO. The results obtained are in good agreement with those calculated for the suggested formulae, and the melting point is sharp indicating the purity of the prepared metal complexes.

Molar conductance measurements

The molar conductance values of all metal complexes were obtained in DMF as a solvent at room temperature and their results in (Ω^{-1} mol^{-1} cm^2) are recorded in Table 1. Generally, higher molar conductance values are indicative of the electrolytic nature of all metal complexes except for Mn(II) and Ni(II) complexes [2].

It is concluded from the results given in Table 1 that the Fe(III) and Cr(III) chelates have molar conductivity values of 85 and 87 Ω^{-1} mol^{-1} cm^2, respectively, indicating that they are 1:1 electrolytes. The molar conductivity values of Fe(II), Co(II), Cu(II) and Zn(II) chelates under investigation (Table 1) are found to be 120, 130, 145 and 140 Ω^{-1} mol^{-1} cm^2, respectively. It is obvious from these data that these chelates are ionic in nature and they are of the type 1:2 electrolytes. Mn(II) and Ni(II) chelates showed their molar conductance values fall in the range of 16–20 Ω^{-1} mol^{-1} - cm^2 indicative of their non-electrolytic nature [1,2].

IR spectral studies

The IR spectra of the complexes are compared with those of the parent drug in order to determine the coordination sites that may be involved in chelation. There are some guide peaks, in the spectrum of the free ligand, which are of great help for achieving this goal. The position and/or the intensities of these peaks are expected to be changed upon complex formation [9]. The characteristic peaks of the free ligand and its metal complexes are listed in Table 2.

Upon comparison the spectrum of the free LOR ligand showed a broad band at 3436 cm^{-1} which assigned to υ(OH) stretching vibration. This band is still broad in all complexes and exists in the range of 3429–3438 cm^{-1}. The presence of coordinated or hydrated water molecules renders it difficult to attribute the broadness of this band to the involvement of OH group in coordination. The υ(CONH) stretching band appeared at 1640 cm^{-1} in the free LOR ligand. It shows a slight shift to lower (5–12 cm^{-1}) or higher (5–15 cm^{-1}) wave number in the complexes indicating the coordination of the carbonyl group to the metal ions [9–12].

The IR spectrum of the free LOR drug shows a strong band at 1593 cm^{-1} which can assigned to the stretching vibration of the C═N group [13–16]. This band is shifted in the range of (1554–1603 cm^{-1}) upon coordination suggesting the involvement of the lone pair on pyridyl nitrogen in the bond formation with the metal ions [11,15,16]. In addition, C═N bending vibration which appears in LOR drug at 621 cm^{-1} was shifted to 612–635 cm^{-1} in the complexes which support the coordination via the pyridyl nitrogen.

The infrared spectra of the complexes showed new bands at 538–563 and 454–489 cm^{-1} which assignable to ν(M—O) of carbonyl oxygen and ν(M—N) stretching vibrations, respectively, [13,14]. In addition, the bands of coordinated water were observed at 831–887 cm^{-1} and the υ(M—O) stretching vibrations of coordinated water attachment to metal ions are found at 513, 517 and 512 cm^{-1} for Co(II), Cu(II) and Zn(II) complexes, respectively, [9–14]. Furthermore, strong evidence for the presence or absence of coordinated or hydrated water was supported by the thermal analysis studies of these complexes.

Therefore, it is concluded from the IR spectra that LOR behaves as neutral bidentate ligand coordinated to the metal ions via the carbonyl oxygen and pyridyl nitrogen in accordance with the previously published data on similar types of oxicam drugs [11,15–21].

^1H NMR spectra

The ^1H NMR spectra of LOR drug and its $[Zn(LOR)_2(H_2O)_2](BF_4)_2 \cdot H_2O$ complex were recorded in DMSO-d_6 taking TMS as internal standard. The uncoordinated pure LOR has the respective peak positions and corresponding assignments as follows:

Singlet peak at 9.90 ppm (s, 1H) attributed to the OH group and multiplite signals at 7.20–7.90 ppm (m, 5H, pyridine ring and thiophene CH). The characteristic proton signals observed at 4.49 ppm (s, 1H) and 2.93 ppm (s, 3H) are assigned to NH and N—CH_3 groups, respectively.

^1H NMR spectrum of $[Zn(LOR)_2(H_2O)_2](BF_4)_2 \cdot H_2O$ complex shows three signals at 9.95, 4.48 and 2.98 ppm, respectively, assignable to the proton of OH, protons of NH and N—CH_3 groups, respectively, indicating that these groups play no part in coordination.

On comparing the peaks of the free LOR ligand and its complex, it was observed that pyridine protons exhibit a shift at 7.03–7.91 ppm leading to an observation that LOR coordinates to the metal ions through the nitrogen of pyridine ring [11,15,16,22].

Mass spectral studies

The electron impact mass spectra of the $[Mn(LOR)_2(Cl)_2] \cdot H_2O$ (Supplementary Fig. 2) and $[Ni(LOR)_2(Cl)_2]$ (Supplementary Fig. 3) complexes showed the molecular ion peaks at m/z 902 (M+) and 872 (M+) amu, respectively, which confirm the stoichiometry as being of $[ML_2]$ type of these complexes. The proposed formula was confirmed also by showing a peak at 370.80 amu corresponding to the LOR ligand moiety $[(C_{13}H_{10}ClN_3O_4S_2)$ atomic mass 371.80 amu]. The observed peaks were in good agreement with their proposed formulae as indicated by the microanalytical data. Thus, the mass spectral data support the conclusions drawn from the analytical and low molar conductivity values.

UV–Vis absorption studies

To understand the electronic structure of LOR metal complexes, UV–Vis spectra were recorded for these complexes (in DMF) in the range of 200–700 nm. The absorption band observed at 373 nm for the LOR ligand is attributed to n–π^* transition between lone-pair electrons of the p orbital of the N atom in the (HN═CO) group and pyridine ring [23]. The sharp peak found at 294 nm was assigned to π–π^* transition of pyridine and thiophene rings. In the UV–Vis spectra of the metal complexes, the band of the high wavelength side shows slight bathochromic or hypsochromic shift of absorption band relative to its free LOR ligand in a range between 365 and 392 nm. The absorption band at 294 nm in free LOR ligand is changed a little bit in intensity and slightly shifted for metal complexes.

The absorption shift and intensity change in the spectra of the metal complexes most likely originate from the metalation which increases the conjugation and delocalization of the whole electronic system and results in the energy change of the π–π^* and n–π^* transition of the conjugated chromospheres [23–27]. The results clearly indicate that the ligand coordinates to Cr(III), Mn(II), Fe(II), Fe(III), Co(II), Ni(II), Cu(II) and Zn(II) ions, in accordance with the results of the other spectral data. Furthermore, according to modern molecular orbital theory [28], any factors that can influence the electronic density of conjugated system must result in the bathochromic or hypsochromic shift of absorption bands. Here, in case of the metal complexes with the same ligand, the main reason of these shifts is generally related with the electronegativity of the different metal ions [24,28].

Electronic spectra and magnetic moment measurements

The electronic absorption spectra provide reliable information about the ligand arrangement in transition metal complexes. It also serves as a useful tool to distinguish among the square-planar, octahedral or tetrahedral geometries of the complexes [29].

The magnetic moment value of 3.30 B.M. for the Cr(III) complex suggested an octahedral geometry [30]. The prominent electronic spectral bands at 28,960, 26,940 and 13,530 cm^{-1} for $^4A_{2g}(F) \rightarrow {}^4T_{2g}(F)$, $^4A_{2g}(F) \rightarrow {}^4T_{2g}(F)$ and $^4A_{2g}(F) \rightarrow {}^4T_{2g}(P)$ transitions, respectively, also pointed to an octahedral geometry. The magnetic moment measurement of the Mn(II) complex (5.26 B.M.) lies in the range of octahedral geometry [31–35]. The spectrum of Mn(II) complex shows three medium intensity bands at 27,450, 21,660 and 15,470 cm^{-1} which can be assigned to $^4T_{1g} \rightarrow {}^6A_{1g}$, $^4T_{2g}(G) \rightarrow {}^6A_{1g}$ and $^4T_{1g}(D) \rightarrow {}^6A_{1g}$ transitions, respectively, for Mn(II) ion in an octahedral field [33–35]. The electronic absorption spectra of Fe(II) and Fe(III) complexes show three weak bands at (19,450 and 20,100), (21,249 and 21,290) and (26,254 and 25,120) cm^{-1}, which may be assigned to the transitions $^6A_{1g} \rightarrow T_{2g}(G)$, $^6A_{1g} \rightarrow {}^5T_{1g}$ and charge transfer, respectively. The electronic transitions together with the magnetic moment values of 5.01 and 5.33 B.M for Fe(II) and Fe(III) complexes, respectively, suggested an octahedral geometry for these complexes [31–35].

The appearance of three bands in the electronic spectra of Co(II) complex at 22,111, 15,240 and 12,832 cm^{-1} may be assigned to $^4T_{1g}(F) \rightarrow {}^4T_{2g}(F)$, $^4T_{1g}(F) \rightarrow {}^4A_{2g}(F)$ and $^4T_{1g}(F) \rightarrow {}^4T_{1g}(P)$ transitions, respectively [30,35,36]. Also, the Ni(II) complex exhibits four electronic spectral bands at 26,511, 20,686, 14,780 and 13,121 cm^{-1} which may be assigned to charge transfer (LMCT), $^3A_{2g}(F) \rightarrow {}^3T_{2g}(F)$, $^3A_{2g}(F) \rightarrow {}^3T_{1g}(F)$ and $^3A_{2g}(F) \rightarrow {}^3T_{1g}$ transitions, respectively. The position of these bands suggested an octahedral geometry around the Co(II) and Ni(II) ions [29,34–38]. The Cu(II) complex shows broad bands at 24,813 and 13,441 cm^{-1} which may be described to $^2B_{1g} \rightarrow {}^2B_{2g}$, $^2B_{1g} \rightarrow {}^2E_g$ and $^2B_{1g} \rightarrow {}^2A_{1g}$ transitions, and attributed to an octahedral geometry around the Cu(II) ion [30–38]. Furthermore, it shows a broad band at 28,216 cm^{-1} which was assigned to ligand–metal (LMCT) charge transfer excitation. The Co(II), Ni(II) and Cu(II) complexes are found to have magnetic moment values of 5.39, 3.23 and 1.70 B.M., respectively, ensuring the octahedral geometry. The Zn(II) complex is diamagnetic. According to the empirical formula, an octahedral geometry was proposed for this chelate.

ESR studies

From the elemental analysis, electronic and magnetic measurements, it is expected that the complexes behave as octahedral geometry for chloride and borate complexes. Four complex examples were taken for ESR investigation as additional proof to confirm the structure for the complexes [39].

ESR spectrum of $[Cu(LOR)_2(H_2O)_2](BF_4)_2{\cdot}4H_2O$ complex was recorded in the solid state at 25 °C (Fig. 4). The spectrum exhibited two bands, one of them is sharp with $g_{||} = 2.255$ and the other is at $g_{\perp} = 2.166$. The shape of the spectrum is consistent with the octahedral geometry around Cu(II) center in the complex. In axial symmetry, the g-values are related by the expression, $G = (g_{||}-2)/(g_{\perp}-2) = 4$, which measures the exchange interaction between copper(II) centers in the solid. According to Hathaway [39,40], if the value of G is greater than four, the exchange interaction between copper(II) centers in the solid state is negligible, whereas when is less than four, a considerable exchange interaction is indicated in the solid complex. The calculated G value is lower than four ($G = 1.536$) suggesting that there are copper–copper exchange interactions. The observed spectral parameters show the trend $g_{||}$ (2.255) > $g_{\perp}$ (2.166) > g_e (2.0023) which confirm that the unpaired electron is localized in the dx^2-y^2 orbital of the Cu(II) ion in complexes and it is the characteristic of an octahedral geometry [41].

Kivelson and Neiman showed that for an ionic environment $g_{||}$ is normally 2.3 or larger, but for covalent environment $g_{||}$ are less than 2.3. The $g_{||}$ value for the Cu(II) complex is 2.255, consequently the environment is essentially covalent. In order to quantify the degree of distortion of the Cu(II) complex, we selected the f factor ($g_{||}/A_{||}$) obtained from the ESR spectra. Although the f factor which is considered as an empirical index of tetrahedral distortion [42], its value ranges between 105 and 135 for square planar complexes, depending on the nature of the coordinated atoms. In the presence of a tetrahedrally distorted structure, the values can be much larger. The g/A value is 142, evidence in support of octahedral structure for Cu(II) complex.

The ESR spectra of the solid Fe(III), Co(II) and Ni(II) complexes at room temperature do not show ESR signal because the rapid spin lattice relaxation of the Fe(III), Co(II) and Ni(II) (Fig. 4) complexes

Table 2
IR spectra (4000–400 cm^{-1}) of LOR and its binary metal complexes.

LOR	$[Cr(LOR)_2Cl_2]Cl$	$[Mn(LOR)_2Cl_2]{\cdot}H_2O$	$[Fe(LOR)_3](BF_4)_2$	$[Fe(LOR)_2Cl_2]Cl{\cdot}2H_2O$	$[Co(LOR)_2(H_2O)_2](BF_4)_2{\cdot}3H_2O$	$[Ni(LOR)_2Cl_2]$	$[Cu(LOR)_2(H_2O)_2](BF_4)_2{\cdot}4H_2O$	$[Zn(LOR)_2(H_2O)_2](BF_4)_2{\cdot}H_2O$	Assignment
3436br	3435br	3429br	3438br	3437br	3431br	3435br	3435br	3438br	OH stretching
1640sh	1651s	1635s	1632s	1645w	1628s	1635s	1633s	1655s	CONH stretching
1593sh	1597s	1585s	1569s	1603s	1571s	1554s	1574s	1574s	C=N stretching
1330sh	1333sh	1334s	1338s	1348sh	1336s	1335s	1336s	1335s	SO_2 asym
1037s	1039s	1043s	1042s	1040s	1044s	1044s	1047s	1044s	SO_2 sym
621s	–	615s	633s	632s	629	628s	635s	612s	C=N bend
–	538s	547s	559s	563s	548s	551s	552s	548s	M—O stretching
–	–	–	–	–	513s	–	517s	512s	M—O stretching of coordinated water
–	459s	489s	463s	472s	454s	468s	462s	455s	M—N stretching
–	–	–	–	–	887s, 834s	–	876s, 831s	876s, 833s	H_2O stretching of coordinated water

sh = Sharp, m = medium, br = broad, s = small, w = weak.

which broadness the lines at higher temperatures [43,44]. The ESR spectra only show signals that may be accounted for the presence of free radicals that can resulted from the cleavage of any double bond and distribution of the charge on the two neighbor atoms.

Powder X-ray diffraction spectroscopy

To obtain further evidence about the structure of the metal complexes, X-ray powder diffraction was performed [2]. The XRD patterns indicate crystalline nature for Mn(II), Ni(II), Cu(II) and Zn(II) complexes only. It can be easily seen that the pattern of LOR differs from its metal complexes, which may be attributed to the formation of a well-defined distorted crystalline structure. Probably, this behaviour is due to the incorporation of water molecules into the coordination sphere.

Thermal analysis studies

Several reports in the literature demonstrate the importance of thermal analysis by thermogravimetry (TG) and differential thermal analysis (DTA) in the characterization, polymorphism identification, purity evaluation of drugs, compatibility studies for the pharmaceutical formulation, stability and drugs thermal decomposition [45]. Thermal gravimetric analysis (TG) was used as a probe to proof the associated water or solvent molecules to be in the coordination sphere or in the crystalline form [23]. Thermogravimetric (TG) was carried out for the complexes. The stages of decomposition, temperature ranges, decomposition product loss as well as the found and calculated weight loss percentages of the complexes are given in Table 3.

The thermal decomposition process of the LOR drug involves two decomposition steps. Decomposition of the LOR drug started at 185 °C and finished at 670 °C with two stages. The first stage of decomposition involves the removal of $C_{10}H_9ClN_2OS$ molecule in the 185–370 °C temperature range, and is accompanied by a weight loss of 64.62% (calcd 64.68%). The second stage of decomposition occurs in the 370–670 °C temperature range, corresponding to the loss of the C_3HNO_3S molecule, and is accompanied by a weight loss of 35.36% (calcd 35.23%).

TG curve of the $[Cr(LOR)_2Cl_2]Cl$ complex shows four steps of decomposition. The first stage of decomposition occurs in the 40–225 °C temperature range, corresponding to the loss of $C_8H_6Cl_2S_2$ molecule, and is accompanied by a weight loss of 25.97% (calcd 26.29%). The second stage of decomposition involves the removal of HCl and $C_{10}H_{10}N_2$ molecules in the form of nitrogen or carbon oxide gases in the 225–325 °C temperature range, and is accompanied by a weight loss of 21.17% (calcd 21.35%). While the third and fourth stages involve the removal of $C_6H_4Cl_2N_4O_{6.5}S_2$ molecule in the 325–656 °C temperature range, and is accompanied by a weight loss of 41.60% (calcd 41.15%). The total weight loss amounts to 88.67% (calcd 88.79%) and carbon and chromium oxide were remained as residues.

TG curve of the $[Mn(LOR)_2Cl_2]H_2O$ complex indicates that the complex is thermally stable to 50 °C. Decomposition of the complex started at 50 °C and finished at 800 °C with four stages. The first stage of decomposition occurs in the 50–110 °C temperature range, corresponding to the loss of H_2O molecule, and is accompanied by a weight loss of 2.08%. The second stage of decomposition involves the removal of Cl_2 gas in the 110–180 °C temperature range, and is accompanied by a weight loss of 7.40%. While the last two stages involve the removal of two LOR molecules in the 180–800 °C temperature range, and are accompanied by weight loss of 78.66% (calcd 78.97%).

TG thermogram of the $[Fe(LOR)_3](BF_4)_2$ complex indicates that the complex is started decomposition at 50 °C and finished at 600 °C with three stages. The first stage of decomposition occurs within the temperature range from 50 to 230 °C, corresponding to the loss of $C_{16}H_{23}F_8NO_3$ molecule, and is accompanied by a weight loss of 31.27% (calcd 31.59%). The second stage of decomposition involves the removal of $C_4H_3Cl_3OS$ molecule in the 230–310 °C temperature range, and is accompanied by a weight loss of 15.27% (calcd 15.72%). While the third stage involves the removal of the remaining LOR molecules in the form of nitrogen and carbon oxide gases within the temperature range of 310–600 °C, and is accompanied by a weight loss of 37.70% (calcd 37.46%). The total weight loss amounts to 84.56% (calcd 84.24%) leaving carbon, ferric oxide and boron oxide as residues.

The thermal decomposition process of $[Fe(LOR)_2Cl_2]Cl{\cdot}2H_2O$ complex involves three decomposition steps. Decomposition of the complex started at 60 °C and finished at 640 °C with three stages. The first stage of decomposition involves the loss of uncoordinated H_2O molecule in the 60–140 °C temperature range, and is accompanied by a weight loss of 3.67%. The second stage of decomposition occurs in the 140–380 °C temperature range, corresponding to the loss of $C_{16}H_{20}Cl_2N_2S_2$ molecule, and is accompanied by a weight loss of 43.17%. While the third stage involves the removal of $C_2H_4Cl_3N_2O_{8.5}S_2$ molecule in the temperature range from 380–640 °C, and is accompanied by a weight loss of 37.58% (calcd 37.06%).

TG thermogram of $[Co(LOR)_2(H_2O)_2](BF_4)_2{\cdot}3H_2O$ complex shows four steps of decomposition. The first stage of decomposition occurs in the 30–80 °C temperature range, corresponding to the loss of uncoordinated H_2O molecule, and is accompanied by a weight loss of 5.21%. The second stage of decomposition involves the removal of two coordinated water and two C_2H_2 molecules in the 80–190 °C temperature range, and is accompanied by a weight loss of 8.66%. While the third and fourth stages involve the removal of $C_{15}H_{12}Cl_2F_8N_6O_4S_4$ molecule in the 190–630 °C temperature range, and are accompanied by weight loss of 64.59% (calcd 64.78%).

The thermal decomposition process of the $[Ni(LOR)_2Cl_2]$ complex started at 50 °C and finished at 690 °C with three stages. The first stage of decomposition involves the removal of $C_8H_8Cl_4O_3S_3$ molecule within the temperature range from 50 to 270 °C, and is accompanied by a weight loss of 44.60%. The second and third stages of decomposition occur in the 270–690 °C temperature range, corresponding to the loss of the $C_{18}H_{12}N_6O_4S$ molecule and were accompanied by weight loss of 46.49% (calcd 46.70%).

TGA curve of the $[Cu(LOR)_2(H_2O)_2](BF_4)_2{\cdot}4H_2O$ complex shows three steps of decomposition. The first stage of decomposition occurs in the 30–200 °C temperature range, corresponding to the loss of uncoordinated and coordinated water molecules, and is accompanied by a weight loss of 9.89%. The second, third and fourth stages of decomposition involve the removal of two LOR molecules in the 200–760 °C temperature range, and are accompanied by weight losses of 76.38%.

TG curve of the $[Zn(LOR)_2(H_2O)_2](BF_4)_2{\cdot}H_2O$ complex indicates that the complex is thermally decomposed in three steps in the temperature range from 30 to 610 °C. The first stage of decomposition occurs in the 30–150 °C temperature range, corresponding to the loss of uncoordinated and coordinated water molecules, and is accompanied by a weight loss of 5.34%. The second and third stages of decomposition involve the removal of two LOR molecules in the 150–610 °C temperature range, and were accompanied by weight loss of 80.06%. The total weight loss amounts to 85.40% (calcd 85.37%) leaving zinc and boric oxides as residues.

Kinetics studies

The kinetic parameters were calculated for the complexes in order to know the effect of the structural properties of the LOR ligand and the type of the metal on the thermal behaviour of the

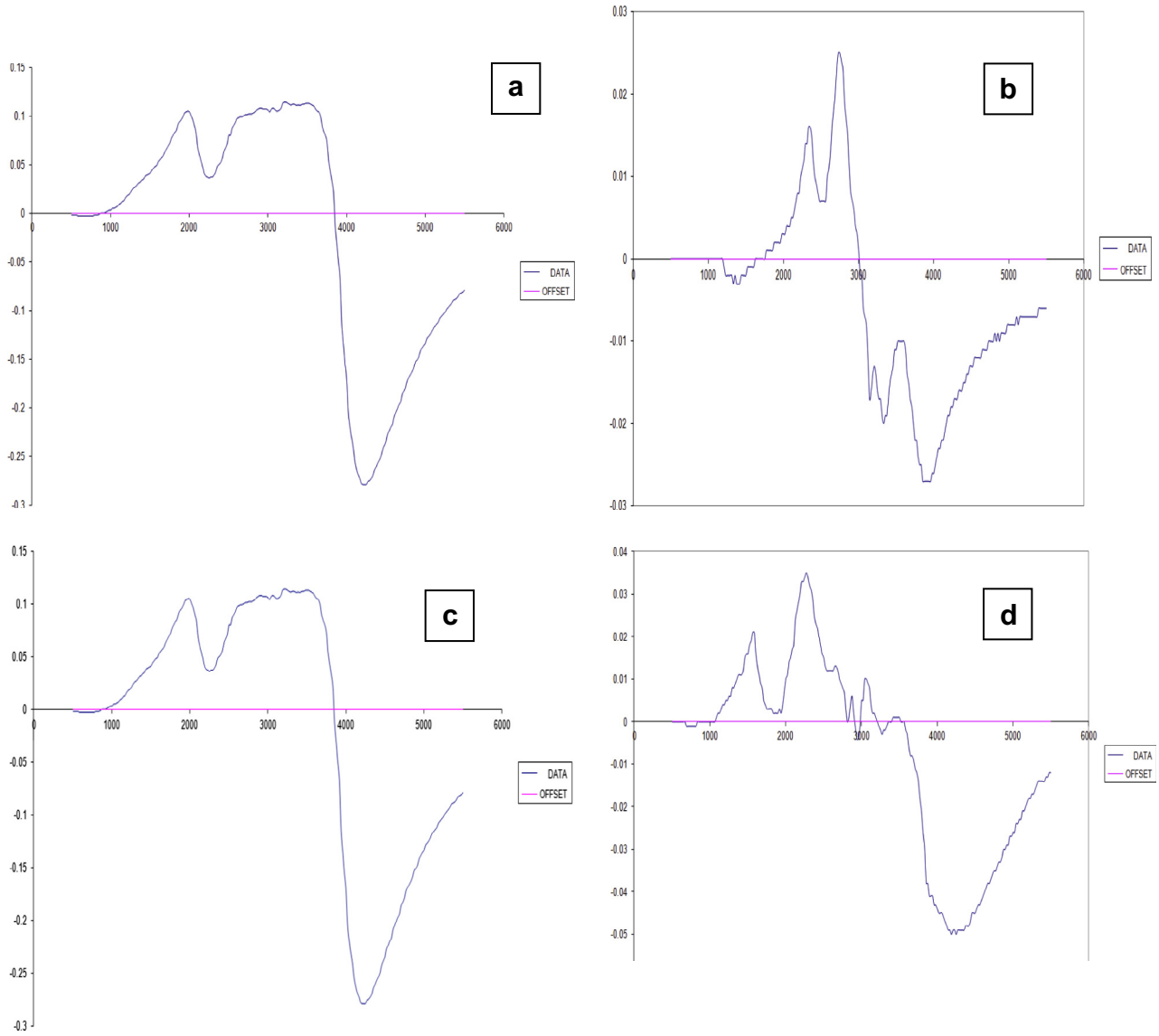

Fig. 4. ESR spectra of some of LOR binary complexes (a) Co(II), (b) Ni(II), (c) Cu(II) and (d) Zn(II) complexes.

complexes and the heat of activation E_a of the various decomposition stages were determined from TG thermograms using the Coats–Redfern [46] and Horowitz–Metzger [47] equations. From the intercept and linear slope of each stage, the A and E_a values were determined. The other kinetic parameters, ΔH^*, ΔS^* and ΔG^* were calculated using the relationships;

$$\Delta H^* = E - \mathrm{RT},$$

$$\Delta S^* = R[2.303\log(\mathrm{Ah}/\mathrm{kt}) - 1]$$

$$\Delta G^* = \Delta H^* - T\Delta S^*$$

where k is the Boltzmann's constant and h is the Planck's constant. The kinetic parameters for the complexes are listed in Supplementary Table 4. The following remarks can be pointed out. The value of ΔG^* increases for the subsequently decomposition stages of a given complex. This is due to increasing the values of $T\Delta S^*$ from one stage to another. Increasing the values of ΔG^* of a given complex as going from one decomposition step to another indicates that the rate of removal of the subsequent ligand will be lower than that of the precedent ligand. This may be attributed to the structural rigidity of the remaining complex after the expulsion of one and more ligands, as compared with the precedent complex, which require more energy, $T\Delta S^*$, for its rearrangement before undergoing any change. The high values obtained for the activation energies reflect the thermal stability of the complexes. The negative values of activation entropies ΔS^* indicate a more ordered activated complex than the reactants and/or the reactions are slow. The positive values of ΔH^* mean that the decomposition processes are endothermic.

Structural interpretation

From all of the above observations, the structure of these complexes may be interpreted in accordance with complexes of LOR drug with a similar distribution of like coordinating sites [11,15,16,48]. The structural information from the previously reported complexes is in agreement with the data reported in this paper based on the IR, ^{1}H NMR, mass, molar conductance, ESR, magnetic and electronic spectra measurements. Consequently, the structures proposed are based on octahedral complexes. The LOR drug always coordinates via the amidic oxygen and the pyridyl nitrogen atoms forming two binding chelating sites. The proposed structural formulas of the above complexes are summarized as three types of coordination as follow:

(a) In case of Co(II), Cu(II) and Zn(II) complexes (where $y = 3$, 4 and 1 for Co(II), Cu(II) and Zn(II) complexes, respectively).

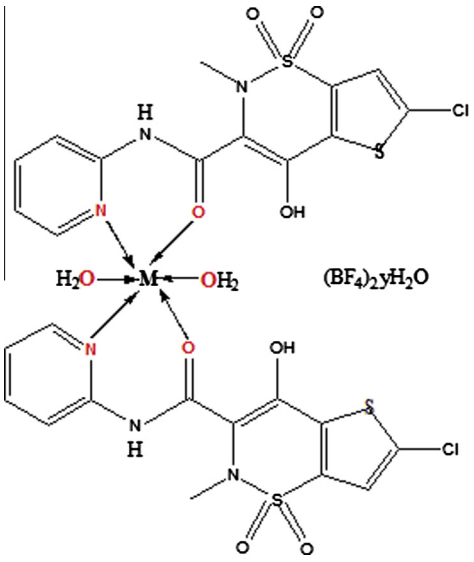

(b) In case of Cr(III), Mn(II), Fe(III) and Ni(II) complexes (where $n = 1$, $y = 0$ for Cr(III) complex, $n = 0$, $y = 1$ for Mn(II) complex, $n = 1$, $y = 2$ for Fe(III) complex and $n = 0$, $y = 0$ for Ni(II) complex).

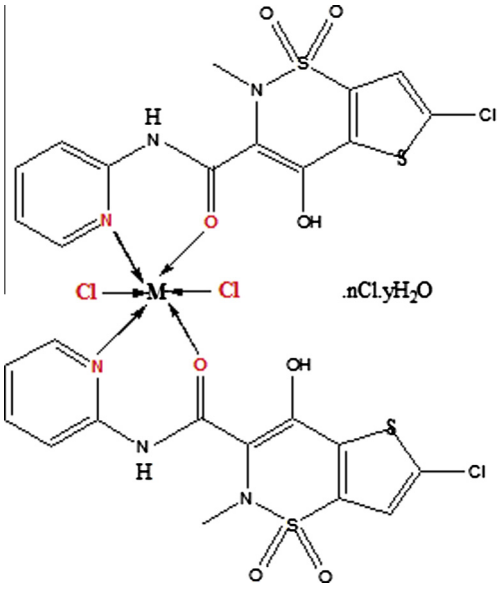

(c) In case of Fe(II) binary complex:

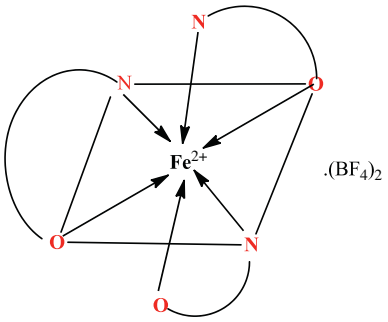

Pharmacology

The LOR drug and its metal complexes were evaluated for antibacterial activity against gram positive, gram negative bacteria and fungi by diffusion agar technique. The zone of inhibition was measured in mm and the values of the investigated compounds are summarized in Table 5. The antimicrobial data reveals that LOR ligand and standards in solution show inhibition capacity much less than the corresponding complexes against all the species under study.

Antifungal activities

The preliminary fungi toxicity screening of the complexes was performed against the photopathogenic fungi *C. albicans* in vitro by the diffusion technique [49]. The inhibition of fungal growths expressed in percentage terms was determined on the growth in test plate compared to the respective control plates as given:

$$\text{Inhibition}\% = 100(C - T)/C$$

(where C, diameter of the fungal growth on the control, T; diameter of the fungal growth on the test plate). All the compounds show no fungal growth inhibition as well as the LOR drug.

Antibacterial activities

The antibacterial action of the LOR ligand and its metal(II)/(III) complexes was checked by disk diffusion method [50]. This was done by the bacterial species *B. subtilis*, *S. aureus*, *N. gonorrhoeae* and *E. coli*. The bacterial growth inhibitory capacity of the ligand and its complexes follow the order Cr(III)=Co(II)=Cu(II)=Zn(II) > Fe(II)=Ni(II) > Amikacin > LOR=Mn(II)=Fe(III) (for *B. subtilis*); Fe(II) > Cr(III) > Fe(III)=Co(II)=Cu(II)=Zn(II) > LOR=Ni(II)=Amikacin > Mn(II) (for *S. aureus*), Zn(II) > Fe(II) > Cr(III)=Co(II)=Cu(II) > LOR=Fe(III)=Ni(II) > Amikacin > Mn(II) (for *N. gonorrhoeae*) and Cr(III) > Fe(II)=Co(II)=Cu(II) > Fe(III)=Ni(II)=Zn(II) > Amikacin > LOR=Mn(II) (for *E. coli*) given in the (Fig. 5).

From the observed result, metal complexes showed enhanced antimicrobial activity in many cases over the free LOR ligand and standards. Such increased activity of the metal complexes can be explained on the basis of chelation theory [51]. This would suggest that the chelation could facilitate the ability of a complex to cross a cell membrane and can be explained by Tweedy's chelation theory [52]. The pathogens secreting various enzymes, which are involved in the breakdown of activities, appear to be especially susceptible to inactivation by the ions of complexes. The metal complexes facilitate their diffusion through the lipid layer of spore membrane to the site of action and ultimately killing them by combining with the OH, SO_2 and C=N groups of certain cell enzymes. The Cr(III), Co(II), Fe(II), Cu(II) and Zn(II) complexes show greater antibacterial activity towards bacteria [Fig. 5]. The variation in the activity of the metal complexes against different organisms depends on the impermeability of the microorganism cells or on differences in ribosome of microbial cells [52].

The complexation with metal(II)/(III) ions can somewhat increase the activities of LOR against Gram-positive more than Gram-negative bacteria. It is well known that the bacterial cell wall is a good target for antimicrobial agents, metal complexes among them. The latter finding is accounted for, by the fact that the first barrier capable of limiting antimicrobial activities is the outer membrane of Gram-negative bacteria. This fact is widely known and referred to as 'intrinsic resistance' of Gram-negative bacteria.

On the other hand, important characteristics that can be correlated with a good antimicrobial activities are as follows: (i) the presence of uncoordinated groups that permits the recognition by living organism and enhances the solubility (hydrophilic or

Table 3
Thermoanalytical results (TG and DTG) of LOR and its binary metal complexes.

Complex	TG range (°C)	DTG_{max} (°C)	n^*	Mass loss	Total mass loss	Fragment loss	Residues
				Estim (Calcd) %			
LOR	185–370	227	1	64.62 (64.68)	99.98 (99.91)	Loss of $C_{10}H_9ClN_2OS$.	–
	370–670	542	1	35.36 (35.23)		Loss of C_3HNO_3S	
$[Cr(LOR)_2{\cdot}Cl_2]Cl$	40–225	216	1	25.97 (26.29)	88.67 (88.79)	Loss of $C_8H_6Cl_2S_2$.	$2C + ½\ Cr_2O_3$
	225–325	270	1	21.17 (21.35)		Loss of HCl and $C_{10}H_{10}N_2$.	
	325–656	459, 610	2	41.60 (41.15)		Loss of $C_6H_4Cl_2N_4O_{6.5}S_2$.	
$[Mn(LOR)_2{\cdot}Cl_2]{\cdot}H_2O$	50–110	56	1	2.08 (2.03)	88.14 (88.87)	Loss of H_2O.	C + MnO
	110–180	138	1	7.40 (7.99)		Loss of Cl_2.	
	180–800	218, 571	2	78.66 (78.97)		Loss of $C_{25}H_{22}Cl_2N_6O_6S_4$.	
$[Fe(LOR)_3](BF_4)_2$	50–230	209	1	31.27 (31.59)	84.56 (84.24)	Loss of $C_{16}H_{23}F_8N_3O$.	$5C + ½\ Fe_2O_3 + B_2O_3$
	230–310	282	1	15.27 (15.72)		Loss of $C_4H_3Cl_3OS$.	
	310–600	498	1	37.70 (37.46)		Loss of $C_{14}H_4N_6O_{5.5}S_5$.	
$[Fe(LOR)_2{\cdot}Cl_2]$	60–140	80	1	3.67 (3.68)	84.42 (84.92)	Loss of $2H_2O$.	$6C + ½\ Fe_2O_3$
$Cl{\cdot}2H_2O$	140–380	218	1	43.17 (43.66)		Loss of $C_{16}H_{20}Cl_2N_2S_2$.	
	380–640	472	1	37.58 (37.06)		Loss of $C_2H_4Cl_3N_2O_{8.5}S_2$.	
$[Co(LOR)_2{\cdot}(H_2O)_2]$	30–80	41	1	5.21 (5.06)	78.46 (78.48)	Loss of $3H_2O$.	$7C + CoO + B_2O_3$
$(BF_4)_2{\cdot}3H_2O$	80–190	95	1	8.66 (8.63)		Loss of $2H_2O$ and two C_2H_2.	
	190–630	218, 555	2	64.59 (64.78)		Loss of $C_{15}H_{12}Cl_2F_8N_6O_4S_4$.	
$[Ni(LOR)_2{\cdot}Cl_2]$	50–270	212	1	44.60 (44.64)	91.09 (91.34)	Loss of $C_8H_8Cl_4O_3S_3$.	NiO
	270–690	397, 499	2	46.49 (46.70)		Loss of $C_{18}H_{12}N_6O_4S$.	
$[Cu(LOR)_2(H_2O)]\ (BF_4)_2{\cdot}4H_2O$	30–200	98	1	9.89 (9.92)	86.27 (86.23)	Loss of $6H_2O$.	$CuO + B_2O_3$
	200–760	260,516, 603	3	76.38 (76.31)		Loss of $C_{26}H_{20}Cl_2F_8N_6O_4S_4$.	
$[Zn(LOR)_2(H_2O)_2]$	30–150	130	1	5.34 (5.21)	85.40 (85.37)	Loss of $3H_2O$.	$ZnO + B_2O_3$
$(BF_4)_2{\cdot}H_2O$	150–610	209, 610	2	80.06 (80.16)		Loss of $C_{26}H_{20}Cl_2F_8N_6O_4S_4$.	

n^* = Number of decomposition steps.

Table 5
Biological activity of LOR ligand and its metal complexes.

Sample	Inhibition zone diameter (mm/mg sample) ± SD				
	Bacillus subtilis	*Staphylococcus aureus*	*Neisseria gonorrhoeae*	*Escherichia coli*	*Candida albicans*
Control: DMSO	0	0	0	0	0
LOR	0	9 ± 0.06	9 ± 0.03	0	0
$[Cr(LOR)_2Cl_2]Cl$	10 ± 0.05	11 ± 0.04	10 ± 0.06	12 ± 0.06	0
$[Mn(LOR)_2Cl_2]{\cdot}H_2O$	0	0	0	0	0
$[Fe(LOR)_3](BF_4)_2$	9 ± 0.07	12 ± 0.03	11 ± 0.06	10 ± 0.04	0
$[Fe(LOR)_2Cl_2]\ Cl{\cdot}2H_2O$	0	10 ± 0.07	9 ± 0.04	9 ± 0.03	0
$[Co(LOR)_2(H_2O)_2]\ (BF_4)_2{\cdot}3H_2O$	10 ± 0.06	10 ± 0.05	10 ± 0.06	10 ± 0.04	0
$[Ni(LOR)_2Cl_2]$	9 ± 0.03	9 ± 0.04	9 ± 0.03	9 ± 0.06	0
$[Cu(LOR)_2(H_2O)_2]\ (BF_4)_2{\cdot}4H_2O$	10 ± 0.08	10 ± 0.03	10 ± 0.05	10 ± 0.07	0
$[Zn(LOR)_2(H_2O)_2]\ (BF_4)_2{\cdot}H_2O$	10 ± 0.07	10 ± 0.06	12 ± 0.05	9 ± 0.03	0
Amikacin	6 ± 0.04	9 ± 0.06	7 ± 0.03	6 ± 0.06	0
Ketokonazole	–	–	–	–	9 ± 0.04

SD = standard deviation.

hydrophobic), (ii) the ability to form hydrogen bonding with a counter anion or solvent molecules, (iii) the dimension and nature of the substituted groups attached to the donor atoms that influence the LOR ligand lipophilicity and membrane permeability, controlling thus the cell penetration, (iv) the small coordination number or the presence of some ligands easy to be removed in interaction with biomolecules, (v) a stereochemistry that allows a favorable three dimensional interaction with biomolecules and (vi) a high kinetic and thermodynamic stability in order to control the dissociation in the acidic medium from the stomach, the metabolization in sanguine flux and to induce a low substitution rate with the biomolecules.

Anticancer activity evaluation

New studies from the last years revealed that in addition to arthritis and pain, cancer and neurodegenerative diseases like Alzheimer's disease could potentially be treated with COX-2 inhibitors [1,48]. The LOR drug and the binary metal complexes were screened for their activity against breast cancer cell line (MCF7) by using 100 μg/ml drug concentration. From these result, it is clear that metal complexes of Cr(III), Fe(II) and Cu(II) were found to be very active against breast cancer cell with inhibition ratio values between 74% and 86%, while other complexes utilized in this work had been shown to be inactive (less than 70% inhibition). It is clear that a pattern of activity can be determined using different drug concentrations (Table 6) and Fig. 6. The IC_{50} values are found to be 21.8%, 22.1% and 21.8% for Cr(III), Fe(II) and Cu(II) complexes, respectively. The cytotoxic activity shown by these metal complexes against (MCF7) cell line indicates that coupling of LOR to the different metal centers resulted in a metallic complex with important biological properties and remarkable cytotoxic activity, since it displays IC_{50} values in a better range to that of many anti-tumor drugs [1,18]. Thus, these complexes are considered as agent with potential anti-tumor activity and can therefore be candidate for further stages of screening in vitro and/or in vivo.

Thus, our investigation showed that some metal complexes may be more active than the parent LOR drug and Amikacin and ketokonazole standards and they may be of interest in designing new drugs. The tested LOR and its metal complexes showed promising antibacterial and anticancer activities and weak antifungal activity.

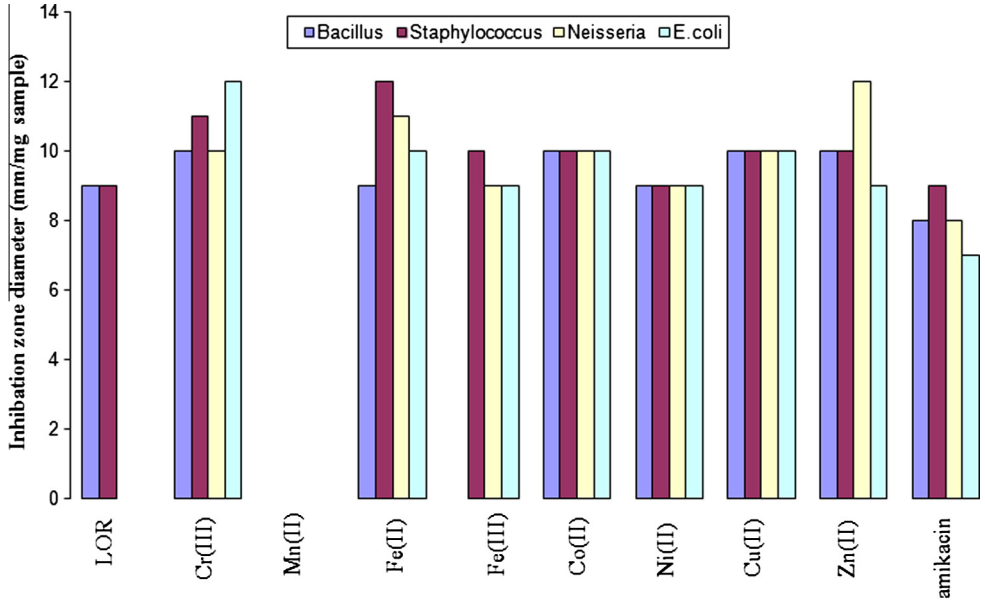

Fig. 5. Biological activity of LOR and its binary complexes.

Table 6
Antibreastic cancer activity of LOR and its binary complexes.

Complex	Concn. (mg/ml)	Surviving fraction (MCF7)					IC_{50} (mg/ml)
		0.0	5	12.5	25	50	
LOR		1.0	1.0	1.0	1.0	1.0	0.0
$[Cr(LOR)_2{\cdot}Cl_2]Cl$		1.0	0.851	0.659	0.446	0.344	21.8
$[Mn(LOR)_2{\cdot}Cl_2]{\cdot}H_2O$		1.0	1.0	1.0	1.0	1.0	0.0
$[Fe(LOR)_3](BF_4)_2$		1.0	0.828	0.723	0.432	0.317	22.1
$[Fe(LOR)_2{\cdot}Cl_2]Cl{\cdot}2H_2O$		1.0	1.0	1.0	1.0	1.0	0.0
$[Co(LOR)_2{\cdot}2H_2O](BF_4)_2{\cdot}3H_2O$		1.0	1.0	1.0	1.0	1.0	0.0
$[Ni(LOR)_2{\cdot}Cl_2]$		1.0	1.0	1.0	1.0	1.0	0.0
$[Cu(LOR)_2(H_2O)_2](BF_4)_2{\cdot}4H_2O$		1.0	0.895	0.746	0.457	0.412	21.8
$[Zn\ (LOR)_2(H_2O)_2](BF_4)_2{\cdot}H_2O$		1.0	1.0	1.0	1.0	1.0	0.0

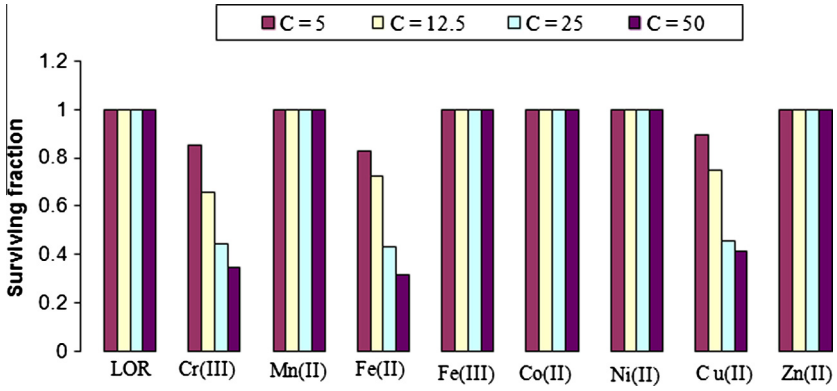

Fig. 6. Anticancer activity of LOR and its binary complexes.

Conclusion

The investigated lornoxicam drug introduced new series of some transition metal complexes having octahedral structures. The solid reflectance spectra show that the metal adopts octahedral coordination. The LOR ligand functions as a neutral bidentate chelate and coordinates to the metal via the C=N (nitrogen atom of pyridine moiety) and oxygen atom of C=O (amide group). The ESR spectra gave good evidence for the proposed structure and the bonding for all studied complexes. Thermal analyses are investigated and allow calculating the kinetic parameters of all thermal decomposition stages of all complexes using Coats–Redfern and Horowitz-Metzger methods. Comparison of the antimicrobial and anticancer activity of the complexes with that of the free LOR drug against different types of bacteria, fungi and MCF7 breast cell line showed promising activity and the possibility of using these metal complexes as drugs in the future is promising target.

Appendix A. Supplementary material

Supplementary data associated with this article can be found, in the online version, at http://dx.doi.org/10.1016/j.saa.2013.11.069.

References

[1] M. Hanif, Z.H. Chohan, Spectrochim. Acta A 104 (2013) 468–476.
[2] A.M.A. Alaghaz, H.A. Bayoumi, Y.A. Ammar, S.A. Aldhlmani, J. Mol. Str. 1035 (2013) 383–399.
[3] G.G. Mohamed, Spectrochim. Acta A 64 (2006) 188–195.
[4] D. Kovala-Demertzi, J. Organomet. Chem. 691 (2006) 1767–1774.
[5] F. Dimiza, A.N. Papadopoulos, V. Tangoulis, V. Psycharis, C.P. Raptopoulou, D.P. Kessissoglou, G. Psomas, J. Inorg. Biochem. 107 (2012) 54–64.
[6] R. Punith, A.H. Hegde, S. Jaldappagari, J. Fluoresc. 21 (2011) 487–495.
[7] I. Sakiyan, E. Logoglu, S. Arslan, N. Sari, Biometals 17 (2004) 115–120.
[8] P. Skehan, R. Storeng, J. Natl. Cancer Inst. 42 (1990) 1107–1112.
[9] T.A. Yousef, G.M. Abu El-Reash, O.A. El-Gammal, R.A. Bedier, J. Mol. Str. 1035 (2013) 307–317.
[10] M.A. El-Ghamry, A.A. Saleh, S.M.E. Khalil, A.A. Mohammed, Spectrochim. Acta A 110 (2013) 205–216.
[11] M.A. Zayed, F.A. Nour El-Dien, G.G. Mohamed, N.E.A. El-Gamel, Spectrochim. Acta A 64 (2006) 216–232.
[12] Walid M.I. Hassan, M.A. Badawy, Gehad G. Mohamed, H. Moustafa, Salwa Elramly, Spectrochim. Acta A 111 (2013) 169–177.
[13] G. Socrates, Infrared Characteristic Group Frequencies, first ed., John Wiley, New York, 1980.
[14] K. Nakamoto, Infrared and Raman Spectra of Inorganic and Coordination Compound, Wiley, New York, 1978.
[15] M.A. Zayed, F.A. Nour El-Dien, Gehad G. Mohamed, Nadia E.A. El-Game, J. Mol. Str 841 (2007) 41–50.
[16] Gehad G. Mohamed, Spectrochim. Acta A 62 (2005) 1165–1171.
[17] M. Goldstein, M.A. Russell, H.A. Willis, Spectrochim. Acta A 25 (1969) 1275–1285.
[18] H.F. Abd El-Halim, G.G. Mohamed, M.M.I. El-Dessouky, W.H. Mahmoud, Spectrochim. Acta A 82 (2011) 8–19.
[19] A. Galani, M.A. Demertzis, Maciej Kubicki, D. Kovala-Demertzi, Eur. J. Inorg. Chem 9 (2003) 1761–1767.
[20] G.G. Mohamed, M.H. Soliman, Spectrochim. Acta A 76 (2010) 341–347.
[21] C.S. Dilip, V.S. Kumar, S.J. Venison, I.V. potheher, D.R. Subahashini, J. Mol. Str 1040 (2013) 192–205.
[22] F. Hanan, F.A. Abd El-Halim, Nour El-Dien, G. Gehad, A. Mohamed, Nehad Mohamed. J. Therm. Anal. and Calor., 111 (2013) 173–181.
[23] Y.T. Liu, G.D. Lian, D.W. Yin, B.J. Su, Spectrochim. Acta A 100 (2013) 131–137.
[24] S. Yadav, R.V. Singh, Spectrochim. Acta A 78 (2011) 298–306.
[25] L. Guo, S. Wu, F. Zeng, J. Zhao, Eur. Polym. J. 42 (2006) 1670–1675.
[26] Z. Chen, Y. Wu, D. Gu, F. Gan, Spectrochim. Acta A 68 (2007) 918–926.
[27] V.T. Kasumov, Spectrochim. Acta A 57 (2003) 1649–1662.
[28] C. Leelavathy, S.A. Antony, Spectrochim. Acta A 113 (2013) 346–355.
[29] S. Seth, K.K. Aravindakshan, Spectrochim. Acta A 112 (2013) 276–279.
[30] M.H. Soliman, G.G. Mohamed, Spectrochim. Acta A 91 (2012) 11–17.
[31] A.B.P. Lever, Coord. Chem. Rev. 3 (1968) 119–140.
[32] F.A. Cotton, G. Wilkinson, C.A. Murillo, M. Bochmann, Advanced Inorganic Chemistry, sixth ed., Wiley, New York, 1999.
[33] M.S. Refat, Spectrochim. Acta A 105 (2013) 326–337.
[34] W.M.I. Hassan, M.A. Badawy, G.G. Mohamed, H. Moustafa, S. Elramly, Spectrochim. Acta A 111 (2013) 169–177.
[35] M.M. Al-Ne'aimi, M.M. Al-Khuder, Spectrochim. Acta A 105 (2013) 365–373.
[36] Madiha.H. Soliman, Gehad.G. Mohamed, Spectrochim. Acta A 107 (2013) 8–15.
[37] H.F. Abd El-Halim, G.G. Mohamed, M.M.I. El-Dessouky, W.H. Mahmoud, J. Pharm. Res. 5 (2012) 5084–5092.
[38] Gehad G. Mohamed, M.M. Omar, Amr A. Ibrahim, Eur. J. Med. Chem. 44 (2009) 4801–4812.
[39] B.J. Hathaway, D.E. Billing, Coord. Chem. Rev. 5 (1970) 143–207.
[40] B.J. Hathaway, Struct. Bond. 57 (1984) 55–118.
[41] K.B. Gudasi, S.A. Patil, R.S. Vadavi, R.V. Shenoy, Trans. Met. Chem. 31 (2006) 586–592.
[42] H. Yokoi, A.W. Addison, Inorg. Chem. 16 (1977) 1341–1349.
[43] M.F.R. Fouda, M.M. Abd-el-Zaher, M.M.E. Shadofa, F.A. El Saied, M.I. Ayad, A.S. El Tabl, Trans. Met. Chem. 33 (2008) 219–228.
[44] S.M. Abdallah, G.G. Mohamed, M.A. Zayed, M.S. Abou El-Ela, Spectrochim. Acta A 73 (2009) 833–840.
[45] M.I. Yoshida, E.C.L. Gomes, C.D.V. Soares, A.F. Cunha, M.A. Oliveira, Molecules 15 (2010) 2439–2452.
[46] A.W. Coats, J.P. Redfern, Nature 201 (1964) 68–69.
[47] H.W. Horowitz, G. Metzger, Anal. Chem. 35 (1963) 1464–1468.
[48] G.G. Mohamed, H.F. Abd El-Halim, M.M.I. El-Dessouky, W.H. Mahmoud, J. Mol. Str. 999 (2011) 29–38.
[49] (a) N. Fahmi, M.K. Biyala, R.V. Singh, Trans. Met. Chem. 29 (2004) 681–683; (b) A. Hooda, V.K. Garg, N.K. Sangwan, K.S. Dhindsa, Proc. Natl. Acad. Sci. 66A (1996) 223–227.
[50] (a) N. Raman, A. Kulandaisamy, C. Thangaraj, K. Jeyasubramanian, Trans. Met. Chem. 28 (2003) 29–36; (b) J.R. Anacona, G.D. Silva, J. Chil. Chem. Soc. 50 (2005) 447–450.
[51] Gehad G. Mohamed, Carmen M. Sharaby, Spectrochim. Acta A 66 (2007) 949–958.
[52] (a) B.G. Tweedy, Phytopathalogy 55 (1964) 910–914; (b) S.K. Sengupta, O.P. Pandey, B.K. Srivastava, V.K. Sharma, Trans. Met. Chem. 23 (1998) 349–352.